Advances in communications using optical vortices

Jian Wang

Wuhan National Laboratory for Optoelectronics, School of Optical and Electronic Information, Huazhong University of Science and Technology, Wuhan 430074, Hubei, China (jwang@hust.edu.cn)

Received May 16, 2016; revised August 4, 2016; accepted August 4, 2016;
posted August 5, 2016 (Doc. ID 264787); published September 1, 2016

An optical vortex having an isolated point singularity is associated with the spatial structure of light waves. A polarization vortex (vector beam) with a polarization singularity has spatially variant polarizations. A phase vortex with phase singularity or screw dislocation has a spiral phase front. The optical vortex has recently gained increasing interest in optical trapping, optical tweezers, laser machining, microscopy, quantum information processing, and optical communications. In this paper, we review recent advances in optical communications using optical vortices. First, basic concepts of polarization/phase vortex modulation and multiplexing in communications and key techniques of polarization/phase vortex generation and (de)multiplexing are introduced. Second, free-space and fiber optical communications using optical vortex modulation and optical vortex multiplexing are presented. Finally, key challenges and perspectives of optical communications using optical vortices are discussed. It is expected that optical vortices exploiting the space physical dimension of light waves might find more interesting applications in optical communications and interconnects.

OCIS codes: (060.4510) Optical communications; (060.2605) Free-space optical communication; (060.2330) Fiber optics communications; (050.4865) Optical vortices; (060.4080) Modulation; (060.4230) Multiplexing.
http://dx.doi.org/10.1364/PRJ.4.000B14

1. INTRODUCTION

An optical vortex is an isolated point singularity of an optical field. This type of vortex is ubiquitous in nature and is commonly known as polarization vortex and phase vortex, characterized by polarization singularity and phase singularity, respectively [1–7]. In the past decades, optical vortex beams have been extensively studied in a variety of fields [3–7]. Polarization vortex beams have found interesting uses in sharp focus with super-resolution spots [8], plasmon excitation and tight focusing [9,10], single-molecule spectroscopy [11], lasing machining [12,13], electron and particle acceleration [14], and 3D optical trapping of nanoparticles, especially metallic particles [15]. Phase vortex beams have found potential uses in optical tweezers [16], optical manipulation [17], optical trapping [18], optical spanner [19], optical vortex knots [20], microscopy [21], and quantum information processing [22,23].

Actually, an optical vortex beam is one of the special beams with a complex beam shape linked to space physical dimension of light waves, i.e., spatial polarization/amplitude/phase structures. Recently, the space physical dimension of light waves has been widely explored in fiber optical communications to facilitate substantial increase of transmission capacity and efficient usage of limited frequency resources by a promising technique, i.e., space-division multiplexing (SDM) [24,25]. Few-mode fiber (FMF), multicore fiber (MCF), and few-mode multicore fiber (FM-MCF) are typical candidates used in SDM fiber optical communications [26–28]. Taking FMF as an example, linearly polarized (LP) modes in a weakly guiding fiber are used as orthogonal information carriers for multichannel information multiplexing and transfer. LP modes could be considered as one kind of mode set in the space physical dimension existing in fiber. Similarly, other mode sets such as Laguerre–Gaussian (LG) modes and Bessel modes in free space and vector eigenmodes in fiber, in principle, also could be used in communications. In this scenario, when employing polarization vortex beams or phase vortex beams as other mode sets, communications using optical vortices are achievable. Beyond the aforementioned fields, optical vortex beams have recently seen possible applications in optical communications and optical interconnects. Several proof-of-concept experimental demonstrations of optical communications using optical vortices have been reported in free space and optical fiber [29–32].

This paper will highlight recent advances in communications using optical vortices. Following the brief introduction of two kinds of optical vortices in Section 2, i.e., polarization vortex and phase vortex, Section 3 describes basic concepts and key techniques of communications using optical vortices. Two kinds of methods using optical vortices in communications are introduced, i.e., optical vortex modulation and optical vortex multiplexing. The generation and (de)multiplexing techniques of optical vortex beams are presented. In Section 4, we review recent research progress in free-space communications using optical vortices. In Section 5, we go over recent research progress in fiber communications using optical vortices. A brief discussion is presented in Section 6. Finally, we summarize the paper in Section 7.

2. POLARIZATION VORTEX AND PHASE VORTEX

Polarization Vortex

Polarization is an important property of light. The well-known linear, elliptical, and circular polarizations of light beams (e.g., plane waves and Gaussian beams) are spatially

homogeneous and do not depend on the spatial location in the beam cross section. Recently there has been increasing interest in light beams with spatially variant polarizations. One typical example is a light beam with cylindrical symmetry in polarization. Such a cylindrical vector beam is called a polarization vortex because its polarization is undetermined at the beam center (i.e., polarization singularity), leading to null intensity at the beam center.

Polarization vortex can take different orthogonal states described by spatially variant polarization $\varphi(\theta) = \boldsymbol{P} \bullet \theta + \varphi_0$, where $\boldsymbol{P}$ is the polarization order, θ is the azimuthal angle, and φ_0 is the initial polarization orientation for $\theta = 0$ [33]. Figures 1(a) and 1(b) illustrate two simple polarization vortex beams, i.e., radially polarized beam (TM_{01}) and azimuthally polarized beam (TE_{01}), respectively. One can clearly see the doughnut-shaped intensity profiles due to the polarization singularity with undetermined polarization at the beam center. A polarization vortex beam features different properties compared with a Gaussian beam. For instance, at focus, the polarization orientation of a Gaussian beam is highly complex, resulting in self-aperturing effects, while a radially polarized beam yields an intense and well-defined electric field along the optic axis [4,34].

Phase Vortex

Phase is another important property of light. Phase front, also known as wavefront, is the locus of points (3D surface) characterized by propagation of position with the same spatial phase. A typical plane wave has a planar phase front. A Gaussian beam also has a planar phase front at its beam waist. Recently light beams with a spiral phase front have attracted increasing interest. Because the phase is undefined at the beam center (i.e., phase singularity or screw dislocation), a light beam having a spiral phase front is called a phase vortex with null intensity at the beam center.

A phase vortex having spiral phase front carries orbital angular momentum (OAM). It was shown by Allen in 1992 that light beams with a spiral phase front comprising an azimuthal phase term $\exp(il\theta)$, have an OAM of $l\hbar$ per photon (l, topological charge value; θ, azimuthal angle; $\hbar$, Plank's constant h divided by 2π) [35]. Different from spin angular momentum (SAM) associated with circular polarization taking only two states of $\pm\hbar$, OAM linked to spatial phase structure can take, in principle, theoretically unlimited orthogonal states. Figures 1(c) and 1(d) depict two simple phase vortex beams (phase distribution in the beam cross-section), corresponding to OAM_{+1} ($l = +1$) and OAM_{-1} ($l = -1$), respectively. The doughnut-shaped intensity profiles are clearly shown in Figs. 1(c) and 1(d) because of the phase singularity with an undefined phase at the beam center.

3. BASIC CONCEPTS AND TECHNIQUES OF COMMUNICATIONS USING OPTICAL VORTICES

Figure 2 illustrates the physical dimensions of photons, including frequency/wavelength, time, complex amplitude, polarization, and spatial structure (space). Actually, almost all the basic techniques of light communications are about the manipulation of different physical dimensions of light waves. For example, the wavelength-division multiplexing (WDM) technique employs the frequency/wavelength physical dimension, the time-division multiplexing (TDM) technique uses the time physical dimension, the quadrature amplitude modulation (QAM) scheme exploits the complex amplitude physical dimension, and the polarization-division multiplexing (PDM) technique utilizes the polarization physical dimension. Those modulation schemes and multiplexing techniques have gained great success in fiber optical communications to increase transmission capacity and spectral efficiency [36].

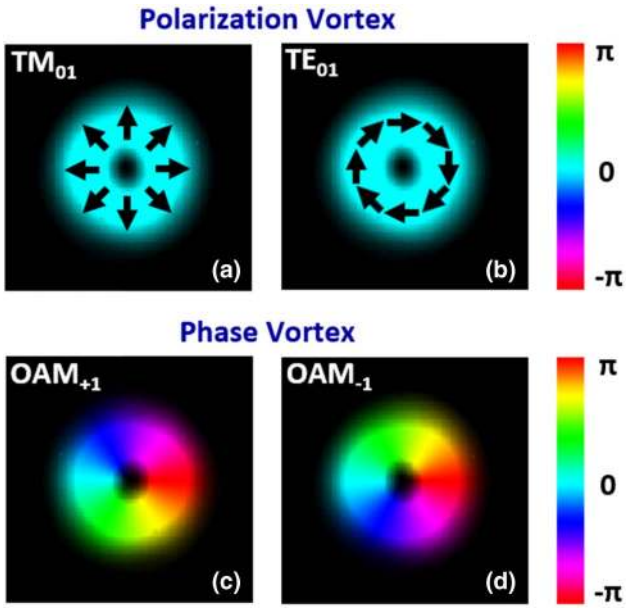

Fig. 1. Schematic illustration of field distributions (polarization, amplitude, phase) of (a,b) polarization vortex and (c,d) phase vortex beams. (a) Radially polarized beam (TM_{01}). (b) Azimuthally polarized beam (TE_{01}). (c) OAM beam with topological charge value of +1 (OAM_{+1}). (d) OAM beam with topological charge value of −1 (OAM_{-1}).

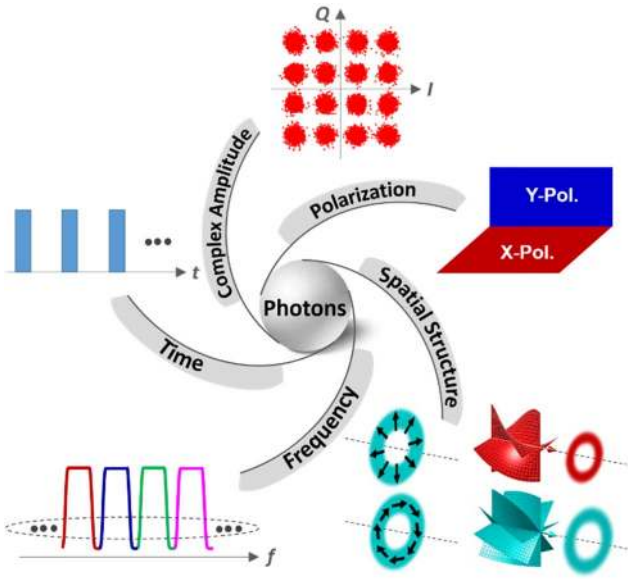

Fig. 2. Schematic illustration of physical dimensions of photons (frequency/wavelength, time, complex amplitude, polarization, spatial structure) and orthogonal states (multiple wavelengths, time slots, constellation points in the complex plane, X- and Y-polarizations, polarization vortices, phase vortices) in modulation schemes and multiplexing techniques.

Meanwhile, it is noted that the similarities in those modulation schemes and multiplexing techniques are the utilization of multiple orthogonal states, which are distinguishable in each physical dimension, i.e., separable wavelengths in WDM, time slots in TDM, constellation points in the complex plane in QAM, and polarizations in PDM. When these traditional physical dimensions are fully exploited, spatial structure physical dimension can be further utilized to enable continuous increase of transmission capacity and spectral efficiency. Similar to other mode sets, optical vortices, i.e., polarization vortices and phase vortices could be candidates for optical communications.

When using optical vortices in communications, similar to other physical dimensions such as frequency, time, complex amplitude, and polarization, we can exploit either optical vortex modulation scheme or optical vortex multiplexing technique. For optical vortex modulation, as depicted in Fig. 3(a), time-varying polarization vortex modulation uses different polarization vortex states to represent different data information. Two polarization vortex states correspond to binary data information (e.g., TM_{01} for "1" and TE_{01} for "0"), while multiple polarization vortex states represent m-ary data information. A similar modulation scheme also can be applied to phase vortex beams, as shown in Fig. 3(b). For optical vortex multiplexing, as shown in Fig. 3(c), different polarization vortex beams (e.g., TM_{01} and TE_{01}) are used as independent carriers to deliver different channel data information. Each channel data information is modulated using the complex amplitude physical dimension such as binary on–off keying (OOK) or m-ary QAM. The multiplexing of multiple channels carried by polarization vortex beams can increase the transmission capacity and spectral efficiency. A similar multiplexing technique also can be applied to phase vortex beams, as depicted in Fig. 3(d). By employing multiple optical vortex beams, it is expected to enable continuous increase of transmission capacity and efficient usage of frequency resources.

For communications using optical vortex modulation and optical vortex multiplexing, one of the most fundamental techniques is optical vortex generation. Polarization vortex beams, also known as vector beams, can be generated using different kinds of schemes, such as active methods using laser intracavity devices that force the laser to oscillate in vector modes [37–39] and passive methods using mode conversion from commonly known spatially homogeneous polarizations into spatially variant polarizations [40,41].

Here we show another simple method to generate polarization vortex beams based on a single phase-only spatial light modulator (SLM) [42]. The experimental setup is shown in Fig. 4. A He–Ne laser at 632.8 nm, a linear polarizer, a neutral density filter (NDF), two lenses, and a pinhole are used to produce a clean collimated Gaussian-like beam (diameter: ~1 cm) with its power controlled and polarization aligned to the working polarization of the SLM (e.g., y direction). To enable polarization vortex beam generation using a single SLM, we divide the SLM into two parts, and the light beam is reflected twice at different areas of the SLM. A compensation phase pattern and a generation phase pattern are loaded to the two divided areas of the SLM. The axis of the half-wave plate (HWM) and the quarter-wave plate (QWP) is rotated by 22.5° and 45° from the y direction, respectively.

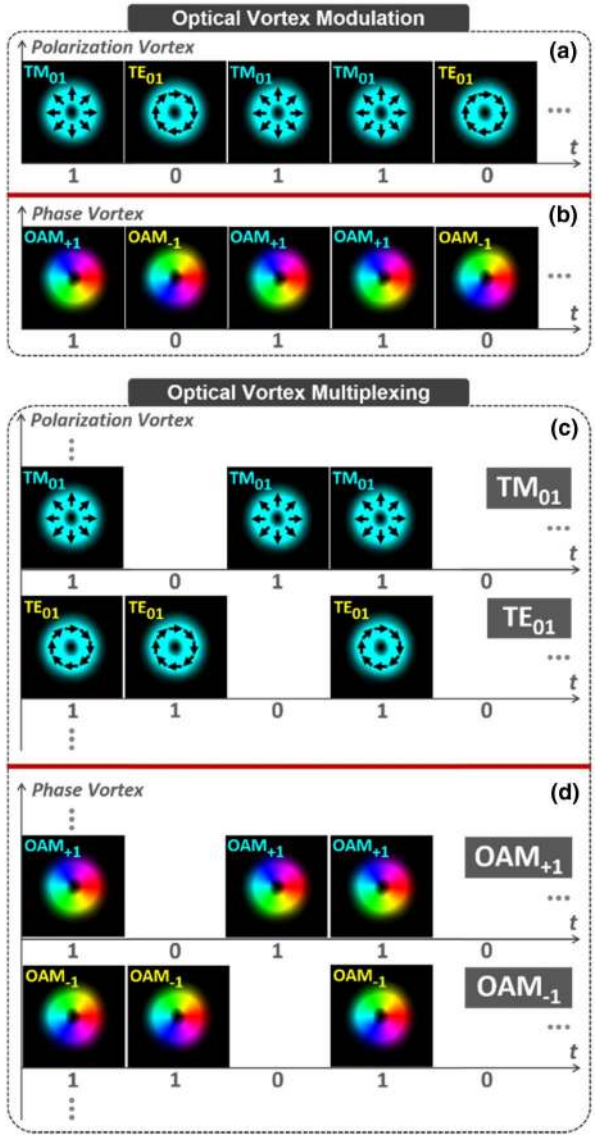

Fig. 3. Schematic illustration of optical vortex modulation and optical vortex multiplexing. (a) Polarization vortex modulation. (b) Phase vortex modulation. (c) Polarization vortex multiplexing. (d) Phase vortex multiplexing.

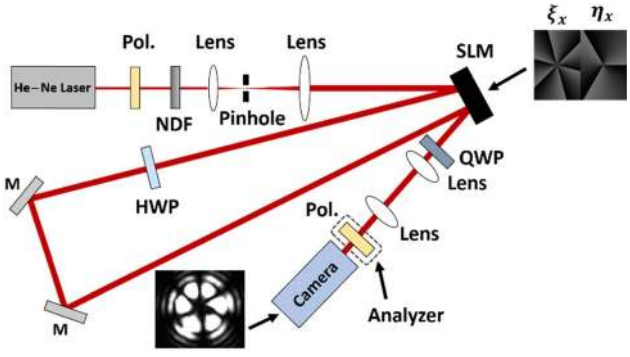

Fig. 4. Experimental setup for generating and detecting polarization vortex beams (radially/azimuthally polarized and high-order vector beams) with a single SLM. Pol., polarizer; M, mirror.

The Jones matrix of the generated polarization vortex beam (vector beam) after the QWP can be expressed as

$$E_{\text{out}} = Q\left(\frac{\pi}{4}\right)M(\xi_{xy})NNH\left(\frac{\pi}{8}\right)M(\eta_{xy})E_{\text{in}} = \frac{1}{2}\exp(-j\eta_{xy})\begin{pmatrix}\sin\xi_{xy}+1+j\cos\xi_{xy}\\ \cos\xi_{xy}+j(1-\sin\xi_{xy})\end{pmatrix}, \quad (1)$$

where $Q(\theta), M(\theta), N$, and $H(\theta)$ are the Jones matrices of QWP, SLM, mirror, and HWP, respectively. $E_{\text{in}} = \binom{0}{1}$ is the Jones vector of the incident light beam. η_{xy} and ξ_{xy} correspond to the phase shift through the first and second reflections by SLM, respectively, which are introduced to the spatial position (x, y) of the light beam. It is proved that the Jones vector in Eq. (1) is linear polarization. Thus one can obtain arbitrary linear polarization at any spatial position (x, y) of the light beam. As a result, the generation of a polarization vortex beam is achievable.

To measure the spatially variant polarization structure and verify the generation of the polarization vortex beam, we record the intensity profiles after the linear polarizer with different orientations. By using four phase patterns shown in Fig. 5(a) loaded to the SLM and adjusting the direction of the linear polarizer, as illustrated in Fig. 5(b), we confirm the successful generation of four different polarization vortex beams, i.e., radially polarized beam with $\boldsymbol{P} = 1$, $\varphi_0 = 0$, azimuthally polarized beam with $\boldsymbol{P} = 1$, $\varphi_0 = \pi/2$, vector beam with $\boldsymbol{P} = 2$, $\varphi_0 = 0$, and vector beam with $\boldsymbol{P} = 3$, $\varphi_0 = 0$, as shown in Figs. 5(c)–5(f). We further demonstrate the generation of 16 polarization vortex beams. The measured multipetal intensity profiles after the linear polarizer are shown in Fig. 6.

Typical methods for the generation of phase vortex beams (i.e., OAM beams) include the use of spiral phase plates (SPPs) [43], cylindrical lens pairs [44], commercially available SLM [45–47], q-plate [48], fiber devices [49–51], photonic integrated devices [52,53], and metamaterials/metasurfaces [54–56]. Most of these methods also could be used in an opposite way for OAM detection. Figure 7(a) shows a typical scheme to generate phase vortex beams using computer-generated spiral phase patterns loaded to the SLM, which converts planar phase fronts (bright spots at beam center) into helical ones (doughnut-shaped intensity profiles). By simply changing the spiral phase patterns, reconfigurable OAM-carrying phase vortex beams are achievable. As shown in Fig. 7(b), inverted spiral phase patterns can back-convert helical phase fronts into planar ones.

We show in Fig. 8 another scheme of phase vortex beam generation, i.e., a controllable all-fiber OAM mode converter. It consists of an FMF with its input port welded with a single-mode fiber (SMF), a mechanical long period grating (LPG), a mechanical rotator, and metal flat slabs. The LPG converts the fundamental fiber mode (LP_{01}) to a higher-order mode (LP_{11}), which is rotated to be 45° with respect to the x and y directions. Variable pressure applied to metal flat slabs induces birefringence between the x and y directions. Proper pressure control can enable a relative $\pm\pi/2$ phase shift between the projected x and y components of 45° rotated

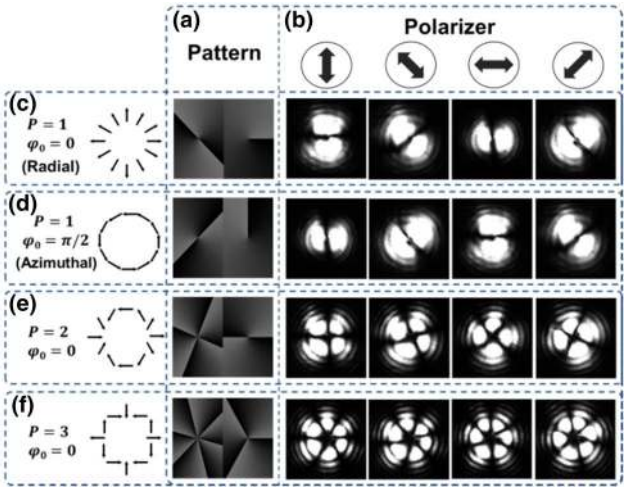

Fig. 5. (a) Phase patterns loaded to SLM for the generation of four polarization vortex beams (radially polarized beam $\boldsymbol{P} = 1$, $\varphi_0 = 0$, azimuthally polarized beam $\boldsymbol{P} = 1$, $\varphi_0 = \pi/2$, vector beam $\boldsymbol{P} = 2$, $\varphi_0 = 0$, vector beam $\boldsymbol{P} = 3$, $\varphi_0 = 0$). (b) Linear polarizer with orientation of 0°, –45°, 90°, 45° with respect to the y direction. (c)–(f) Left column: illustration of spatially variant polarization of four polarization vortex beams. Right four columns: measured multipetal intensity profiles of four polarization vortex beams after linear polarizer.

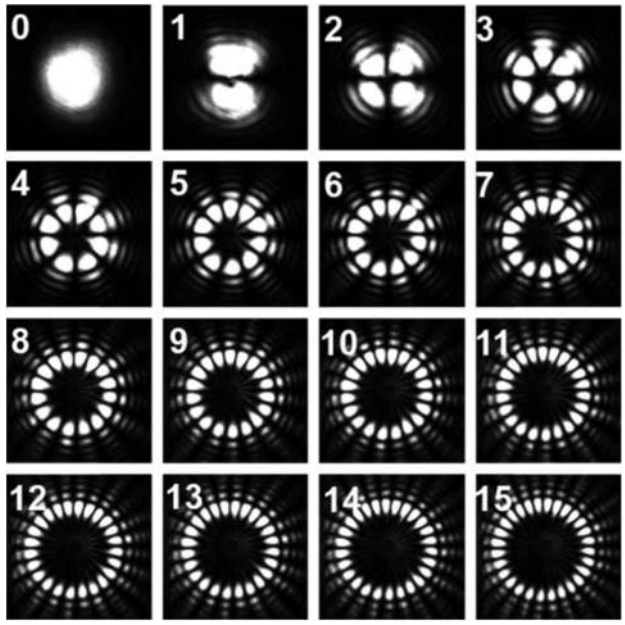

Fig. 6. Measured multipetal intensity profiles of 16 polarization vortex beams after linear polarizer.

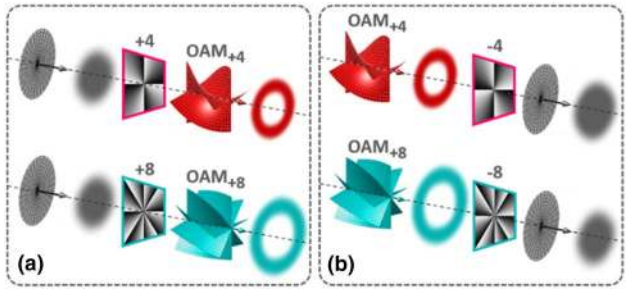

Fig. 7. Schematic illustration of (a) conversion from planar phase fronts to helical ones and (b) backconversion from helical phase fronts to planar ones using spiral phase masks loaded to the SLM.

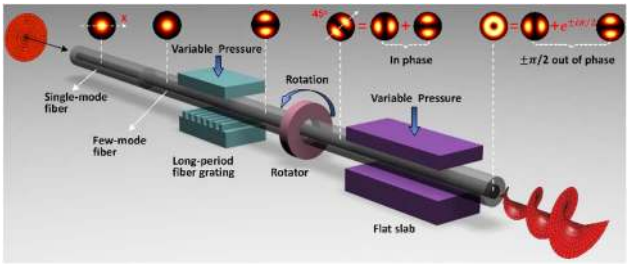

Fig. 8. Schematic illustration of a controllable all-fiber OAM mode converter.

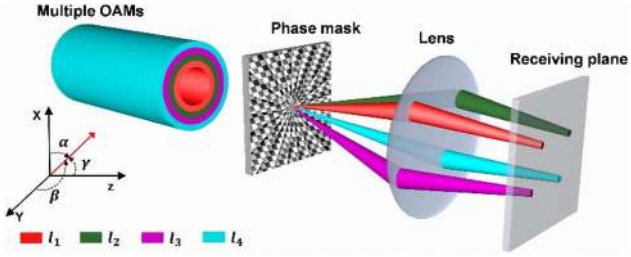

Fig. 10. Schematic illustration of simultaneous demultiplexing and steering of multiple OAM modes using a single complex phase mask.

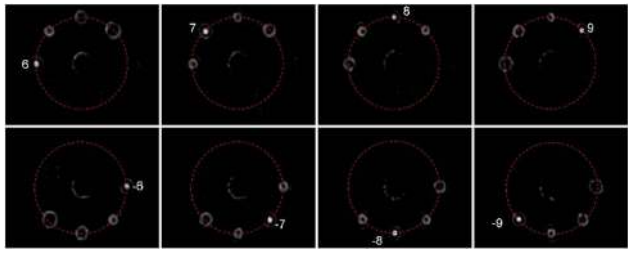

Fig. 11. Measured intensity profiles for the demultiplexing of OAM $l = \pm 6, \pm 7, \pm 8, \pm 9$ with circular-shaped beam steering of demultiplexed beams.

LP_{11} mode, resulting in the generation of OAM-carrying phase vortex beam. Figure 9 shows measured intensity profiles of generated output phase vortex beams and their corresponding interferograms (i.e., interference between phase vortex beams and a reference Gaussian beam). The number of twists and the twist direction determine the topological charge value of the OAM-carrying phase vortex beams. The observed high-quality doughnut-shaped intensity profiles and twisted interferograms indicate successful generation of OAM-carrying phase vortex beams using an all-fiber device, which is compatible with SMF.

In addition to separate generation of either polarization vortex beams or phase vortex beams, combined polarization and phase vortex beams, e.g., OAM-carrying vector beams also could be generated, such as the use of an integrated compact optical vortex emitter with angular gratings inside microrings [57,58] and metamaterials [59].

Remarkably, for communications using optical vortex multiplexing, the commonly used multiplexing devices are cumbersome beam splitters, which are lossy and not scalable. Recently, mode multiplexer based on multiplane light conversion [60], efficient mode sorters based on optical geometric transformations [61,62], complex phase mask [63], Dammann gratings [64], and fiber and photonic integrated devices [65,66] have been proposed as promising candidates for optical vortex (de)multiplexing.

Here we show a simple scheme to perform simultaneous demultiplexing and steering of multiple OAM modes using a single complex phase mask. As illustrated in Fig. 10, by properly designing the complex phase mask, it is possible to perform OAM demultiplexing and also arbitrarily steer the propagation directions of demultiplexed beams. The complex phase mask for multi-OAM (de)multiplexing and steering is constructed by adding multiple fork phase masks (combined helical phase mask and blazed grating phase mask). Shown in Fig. 11 are measured intensity profiles for the demultiplexing of OAM $l = \pm 6, \pm 7, \pm 8, \pm 9$ with circular-shaped beam steering of demultiplexed beams.

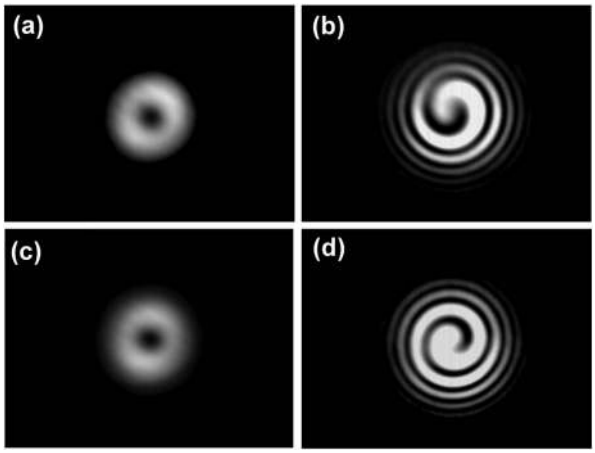

Fig. 9. Measured (a,c) intensity profiles and (b,d) interferograms (interference with reference Gaussian beam) of the generated (a,b) OAM_{-1} and (c,d) OAM_{+1} modes using an all-fiber device.

4. FREE-SPACE COMMUNICATIONS USING OPTICAL VORTICES

The optical vortex modulation scheme and optical vortex multiplexing technique can be both used in optical communications. Shown in Fig. 12 is the concept of free-space communications using polarization vortex modulation [42]. By employing the experimental setup shown in Fig. 4, one can flexibly switch the complex phase pattern loaded to the SLM to generate different polarization vortex beams (vector beams). The multiple orthogonal polarization vortex states can be used to represent high-base numbers, e.g., four states for quaternary numbers, eight states for octal numbers, and 16 states for hexadecimal numbers. The generation and transmission of a time-varying polarization vortex sequence enables free-space data information transfer by polarization vortex modulation. Shown in Fig. 12 is an example of polarization vortex communications using four polarization vortex beams to represent quaternary numbers. At the receiver side, a linear polarizer is used to analyze and determine the states of the received polarization vortex beams and recover the original high-base (e.g., quaternary) number sequence.

We demonstrate the free-space image transfer through a visible-light communication link using polarization vortex modulation. A 64×64 pixels Lena gray image is used in the experiment. The gray value (0–255) of each pixel in the gray image has 1 byte (8 bits) information, corresponding to two

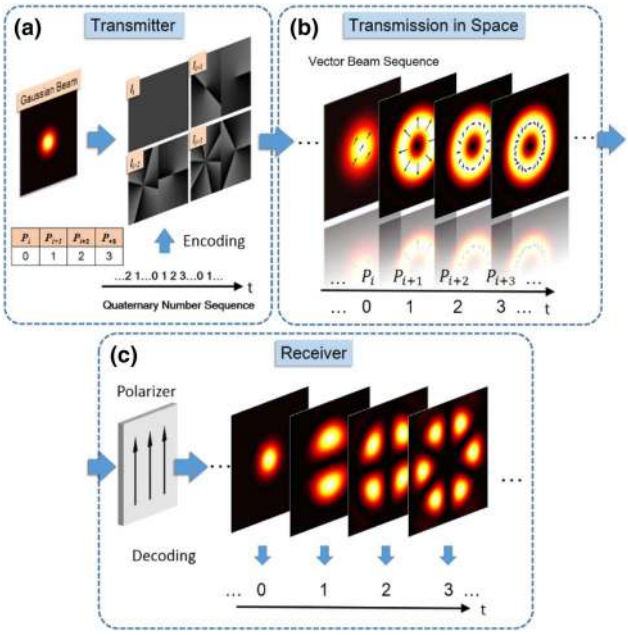

Fig. 12. Schematic illustration of optical communications using polarization vortex modulation.

hexadecimal numbers. Thus a 64×64 pixels Lena gray image can be converted to a sequence with 8192 hexadecimal numbers. Each hexadecimal number is represented by one of 16 polarization vortex states. For example, as shown in Fig. 13, a pixel of the Lena gray image contains 1 byte (8 bits) information, i.e., two hexadecimal numbers $((147)_{10} \rightarrow (93)_{16})$, which are mapped to two 16 states polarization vortex beams with $\boldsymbol{P} = 9$ and $\boldsymbol{P} = 3$, respectively. After free-space information transfer using polarization vortex modulation, a linear polarizer and a camera are used for detection followed by recovery of the received hexadecimal number sequence and corresponding gray image. The transmitted and received 64×64 pixels Lena gray images are shown in Fig. 13. It is found that the received image recovers the transmitted one, which indicates the successful free-space image transfer using polarization vortex modulation. The bit-error rate (BER) performance is evaluated, and zero error among 8192 hexadecimal numbers is observed in the experiment.

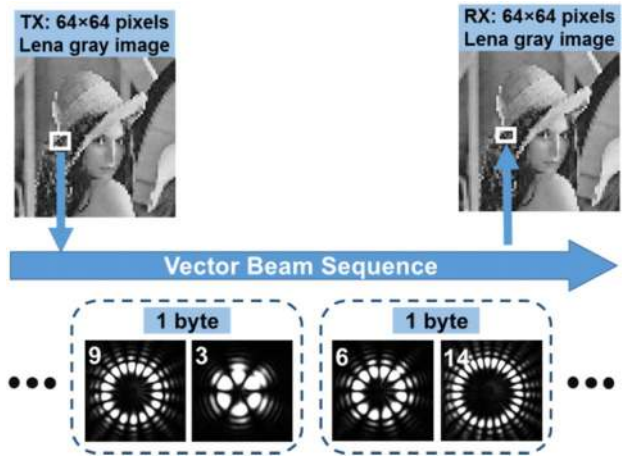

Fig. 13. Free-space 64×64 pixels Lena gray image transfer through a visible-light communication link using polarization vortex modulation.

Polarization vortex beams (vector beams) also can be used to increase the transmission data rate of free-space optical communications via mode-division multiplexing (MDM). One example is polarization vortex multiplexing based on a liquid crystal q-plate [67]. In a proof-of-principle experiment, four vector beams, each carrying a 20 Gbit/s quadrature phase-shift keying (QPSK) (aggregate 80 Gbit/s) on a single wavelength (1550 nm), were transmitted ~1 m with < -16.4 dB mode cross talk. BERs for all vector beams were measured at the 7% forward error correction (FEC) threshold with power penalties <3.41 dB.

In addition to polarization vortex modulation and multiplexing, phase vortex modulation and multiplexing also can be used in optical communications. In 2004, Gibson *et al.* proposed and demonstrated free-space data information transfer using light beams carrying OAM, in which eight switchable OAM beams were generated for OAM coding/decoding [68]. OAM superposition modes transmission over a 3 km intra-city link in Vienna under strong turbulence conditions also were demonstrated [69]. An incoherent detection scheme was employed by directly observing the unambiguous mode-intensity patterns on a screen with the help of a standard adaptive pattern recognition algorithm. Such scheme avoided coherent phase-dependent measurements for identifying the transmitted OAM modes, which was tolerant to atmospheric turbulence. Sixteen different mode superpositions were employed for free-space data information transmission, which were distinguishable with an average error rate of only ~1.7%.

Here we show another example of high-dimensional structured light coding/decoding (OAM-carrying Bessel beams modulation) for free-space optical communications free of obstructions [70]. Shown in Fig. 14 is the schematic illustration of optical communications using phase vortex (OAM-carrying Bessel beam) modulation. Taking four phase vortex states for quaternary numbers as an example, at the transmitter side, each quaternary number corresponds to an OAM-carrying Bessel beam with specific topological charge value (e.g., $0 \rightarrow l_i$, $1 \rightarrow l_{i+1}$, $2 \rightarrow l_{i+2}$, and $3 \rightarrow l_{i+3}$). A quaternary number sequence is mapped to a Bessel beam pattern sequence, which is then added to a Gaussian beam to generate a time-varying Bessel beam sequence for free-space data information transfer. After the transmission in free space, at the receiver side, the OAM-carrying Bessel beam sequence is demodulated by introducing the inverted spiral phase pattern. To demodulate a Bessel beam of $l = l_{i+n}$ $(n = 0, 1, 2, 3)$, four inverted spiral phase patterns $(-l_i, -l_{i+1}, -l_{i+2}, -l_{i+3})$ are employed. It is noted that only one specific inverted spiral phase pattern of $l = -l_{i+n}$ can remove the spiral phase front of the OAM-carrying Bessel beam $l = l_{i+n}$ and convert it to a Gaussian-like beam with a bright spot at the beam center. The demodulation of a Bessel beam of $l = l_{i+n}$ using other inverted spiral phase patterns of $l \neq -l_{i+n}$ still features doughnut-shaped intensity profiles with null spot at the beam center. Therefore, it is possible to determine the Bessel beam and corresponding quaternary number after the demodulation. Similarly, for high-order phase vortex modulation, m Bessel beams of $l = l_i$, $l = l_{i+1}$, $l = l_{i+2} \ldots l = l_{i+m-1}$ can be used to represent m-base numbers $0, 1, 2 \ldots m - 1$, respectively. An m-ary number sequence is transferred to a time-varying Bessel beam sequence

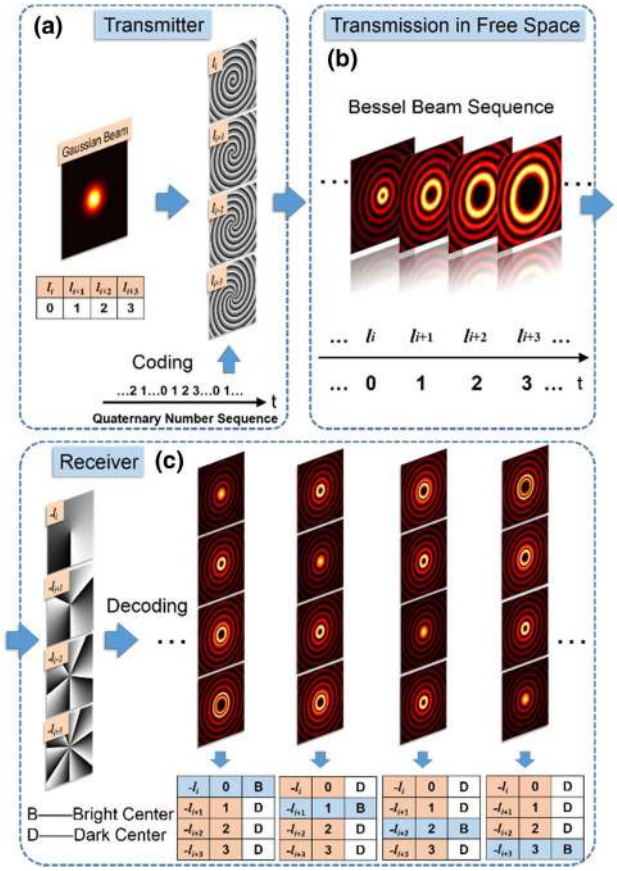

Fig. 14. Schematic illustration of optical communications using phase vortex (OAM-carrying Bessel beam) modulation.

for free-space data information transmission. m inverted spiral phase patterns $(-l_i, -l_{i+1}, -l_{i+2} \ldots -l_{i+m-1})$ are used to demodulate the Bessel beams one by one. Only one inverted spiral phase pattern leads to a bright spot at the beam center. As a result, the transmitted OAM-carrying Bessel beam sequence can be determined, and the corresponding m-ary number sequence can be recovered.

In the experiment, as shown in Fig. 15(a), we first use 16 OAM-carrying Bessel beams of $l = -15, -13, -11 \ldots -1, 1 \ldots 11, 13, 15$ with a channel spacing of $\Delta l = 2$ between adjacent Bessel beams to code 16 hexadecimal numbers $0, 1, 2 \ldots 7, 8 \ldots 13, 14, 15$. Typical decoding results without obstruction are shown in Fig. 15(b). According to the specific inverted spiral phase pattern used to achieve a bright spot at the beam center, one can determine the hexadecimal number of 4, 7, and 15 in Fig. 15(b), respectively. As shown in Fig. 15(c), we then use 32 OAM-carrying Bessel beams of $l = -16, -15, -14 \ldots -2, -1, 1, 2 \ldots 14, 15, 16$ with a channel spacing of $\Delta l = 1$ between adjacent Bessel beam orders to code 32-ary base number $0, 1, 2 \ldots 14, 15, 16, 17 \ldots 29, 30, 31$, respectively. Typical decoding result for 32-ary base number 14 is shown in Fig. 15(d). We further measure the BER performance of free-space data information transfer using phase vortex (OAM-carrying Bessel beam) modulation. The Bessel beam has self-healing properties, i.e., free of obstruction. Figure 16 shows measured BERs for hexadecimal and 32-ary phase vortex modulation without and with obstruction. It is observed that the BER for free-space data information transfer link using hexadecimal phase vortex modulation with $\Delta l = 2$ keeps zero without and with obstruction. In contrast, the BER for free-space communication link using 32-ary phase vortex modulation with $\Delta l = 1$ suffers performance degradations.

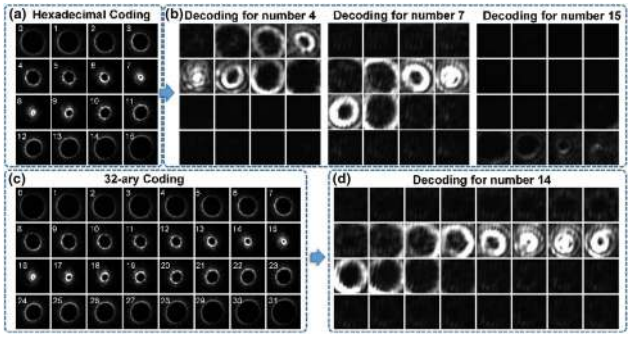

Fig. 15. Measured intensity profiles for free-space data information transfer using phase vortex (OAM-carrying Bessel beam) modulation. (a) Hexadecimal coding. (b) Decoding for hexadecimal number 4, 7, and 15. (c) 32-ary coding. (d) Decoding for 32-ary number 14.

For the phase vortex multiplexing, because the spatial structure physical dimension is compatible with other well-known physical dimensions, the combination of multiple multiplexing techniques is always considered to facilitate the increase of transmission capacity and spectral efficiency. Illustrated in Fig. 17 is the block diagram of free-space optical communications using phase vortex multiplexing combined with other multiplexing techniques, e.g., polarization multiplexing [29]. Multiple data-carrying (e.g., 16 QAM) Gaussian beams are converted to multiple phase vortex beams (e.g., OAM beams) using SLM. Phase vortex multiplexing is realized using a beam splitter or other devices, followed by other multiplexing techniques such as polarization multiplexing. After free-space propagation, the transmitted data signals are detected after polarization demultiplexing and phase vortex demultiplexing.

Here we show recent experiments in free-space optical communications using phase vortex (OAM beams) multiplexing [71–76]. We first demonstrate free-space optical communications using 10 Gbaud 16-QAM signals over four OAM beams (OAM_{-8}, OAM_{+10}, OAM_{+12}, OAM_{-14}). Figure 18 shows

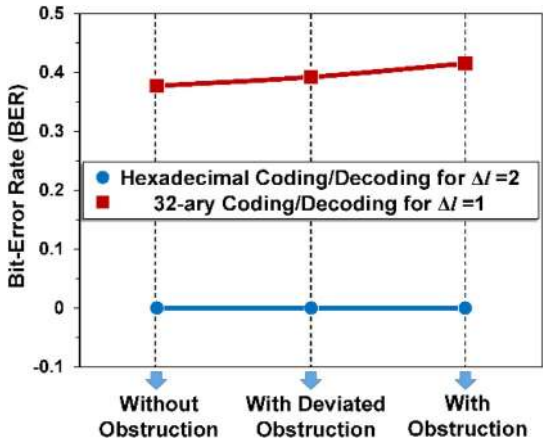

Fig. 16. Measured BER for free-space data information transfer using hexadecimal and 32-ary phase vortex (OAM-carrying Bessel beam) modulation.

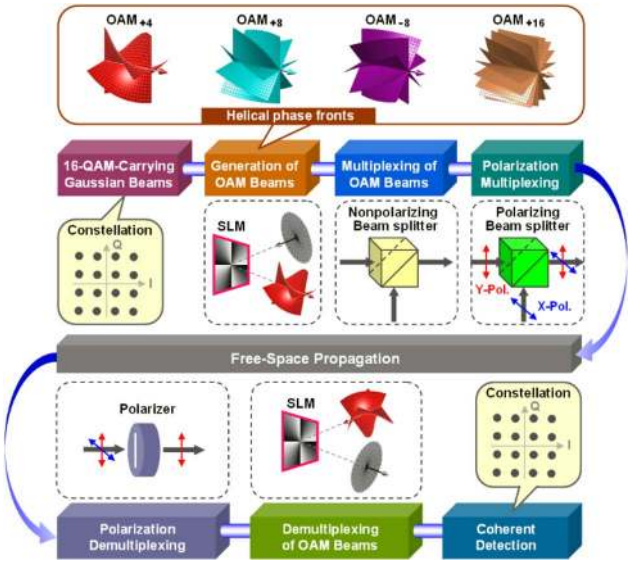

Fig. 17. Schematic illustration of free-space optical communications using phase vortex (OAM beams) multiplexing combined with other multiplexing techniques (e.g., polarization multiplexing).

measured intensity profiles for OAM_{-8}, OAM_{+10}, OAM_{+12}, OAM_{-14}, superposition of four OAM beams and BER performance. One can clearly see the doughnut-shaped intensity profiles of OAM beams. Less than 1.2 and 2.2 dB optical signal-to-noise ratio (OSNR) penalties at a BER of 2×10^{-3} (enhanced FEC [EFEC] threshold) are observed without (w/o) and with (w/) cross talk. Considering 10.7 Gbaud 16-QAM signals over four OAM beams with a 12.5 GHz bandwidth, a spectral efficiency of 12.8 bit/s/Hz, and an aggregate capacity of $171.2(4 \times 4 \times 10.7)$ Gbit/s are achieved, including the 7% FEC overhead.

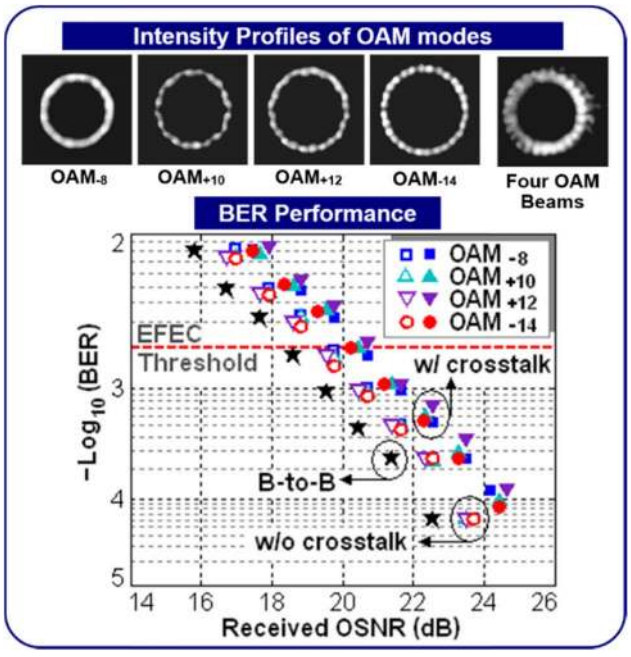

Fig. 18. Measured intensity profiles and BER performance for free-space communications using 10 Gbaud 16-QAM signals over four OAM beams (four channels in total).

We then demonstrate free-space optical communications using 10.7 Gbaud 16-QAM signals over pol-muxed four OAM beams (OAM_{+4}, OAM_{+8}, OAM_{-8}, OAM_{+16}) (12.5 GHz grid). The obtained results are shown in Fig. 19. A spectral efficiency of 25.6 bit/s/Hz and an aggregate capacity of $342.4(4 \times 2 \times 4 \times 10.7)$ Gbit/s are achieved, including the 7% FEC overhead.

We also demonstrate free-space optical communications using 20 Gbaud 16-QAM signals over pol-muxed eight OAM beams (± 10, ± 12, ± 14, ± 16) in two groups of concentric rings (32 channels in total). Shown in Fig. 20 are the measured intensity profile and operation performance. A spectral efficiency of 95.7 bit/s/Hz and an aggregate capacity of 2.56 Tbit/s are obtained. All 32 channels achieve BER less than 2×10^{-3}. The average OSNR penalties for inner and outer rings are 2.7 and 3.6 dB, respectively.

We further demonstrate free-space optical communications using 17.9 Gbit/s orthogonal frequency-division multiplexing (OFDM) offset QAM (OFDM/OQAM) 64-QAM signals over pol-muxed 22 OAM modes (44 channels in total) with a bandwidth of ~3.2 GHz. Figure 21 shows measured intensity profiles of Gaussian beam, pol-muxed 22 OAM modes, y-polarized

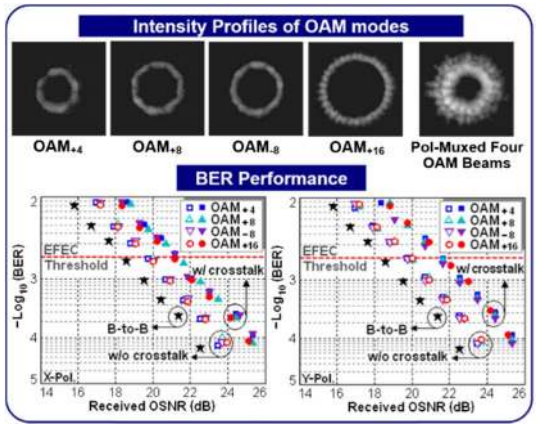

Fig. 19. Measured intensity profiles and BER performance for free-space communications using 10 Gbaud 16-QAM signals over pol-muxed four OAM beams (eight channels in total).

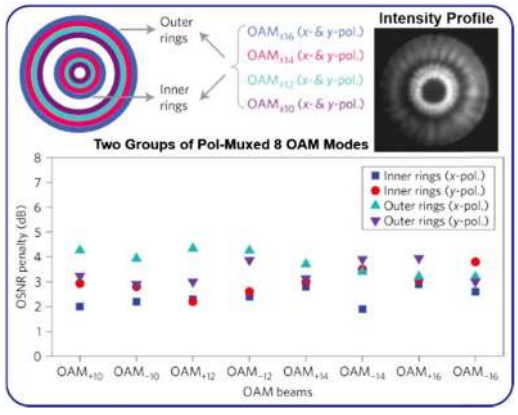

Fig. 20. Measured intensity profile and BER performance for free-space communications using 20 Gbaud 16-QAM signals over pol-muxed eight OAM beams in two groups of concentric rings (32 channels in total).

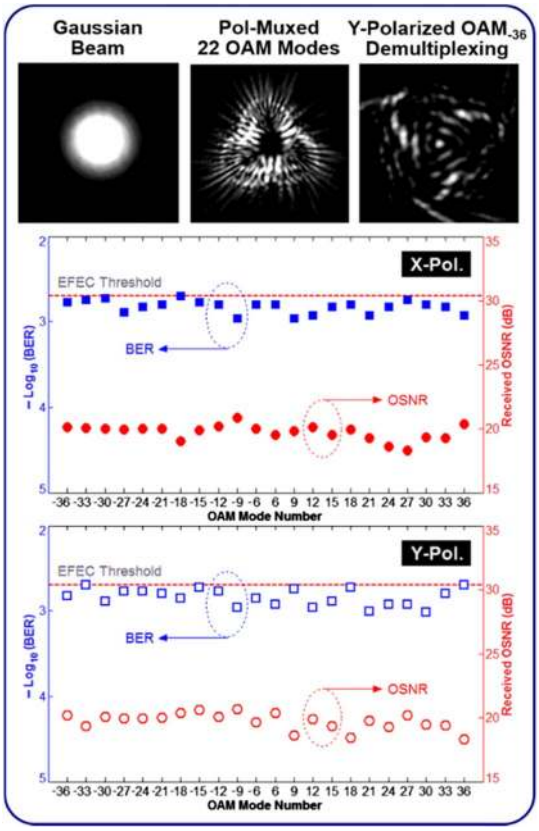

Fig. 21. Measured intensity profiles and BER performance for free-space optical communications using 17.9 Gbit/s OFDM/OQAM 64-QAM signals over pol-muxed 22 OAM modes (44 channels in total).

OAM_{-36} demultiplexing and BER performance. All 44 channels achieve BER less than 2×10^{-3}. A high spectral efficiency of 230 bit/s/Hz is achieved, including the 7% FEC overhead.

Moreover, it is possible to keep increasing the spectral efficiency by exploiting the N-dimensional multiplexing technique. Shown in Fig. 22 is the schematic illustration of N-dimensional multiplexing for increased spectral efficiency. OAM multiplexing, PDM, Nyquist pulse shaping (Nyquist m-QAM signal) are used to enable tremendous increase of spectral efficiency. In the experiment, we demonstrate

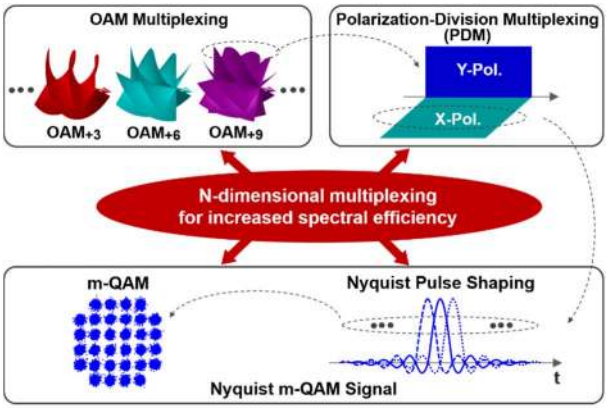

Fig. 22. Schematic illustration of N-dimensional multiplexing for increased spectral efficiency (OAM multiplexing, PDM, Nyquist m-QAM signal).

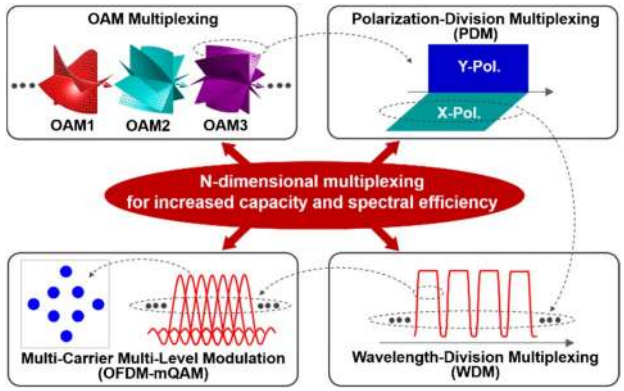

Fig. 23. Schematic illustration of N-dimensional multiplexing for increased transmission capacity and spectral efficiency (OAM multiplexing, PDM, WDM, multicarrier multilevel modulation signal).

free-space optical communications using Nyquist 32-QAM signals over pol-muxed 52 OAM modes and achieve an ultrahigh spectral efficiency of 435 bit/s/Hz.

Remarkably, phase vortex multiplexing also can be combined with the WDM technique to increase spectral efficiency and transmission capacity of optical communications. Using 100 Gbit/s QPSK signals over pol-muxed 12 OAM modes each carrying 42 wavelengths, Huang *et al.* demonstrated free-space optical communications with a total transmission capacity of 100.8 Tbit/s. Shown in Fig. 23 is the schematic illustration of N-dimensional multiplexing for increased transmission capacity and spectral efficiency. OAM multiplexing, PDM, WDM, and a multicarrier multilevel modulation (OFDM-mQAM) signal are used to facilitate increase of transmission capacity and spectral efficiency. In the experiment, using N-dimensional multiplexing (OAM, PDM, WDM, OFDM-mQAM), i.e., 54.139-Gbit/s OFDM-8QAM signals over 368 WDM pol-muxed 26 OAM modes (± 6, ± 9, ± 12, ± 15, ± 18, ± 21, ± 24, ± 27, ± 30, ± 33, ± 36, ± 39, ± 42), we demonstrate free-space optical communications with a total transmission capacity of 1.036 Pbit/s and an aggregate spectral efficiency of 112.6 bit/s/Hz.

5. FIBER COMMUNICATIONS USING OPTICAL VORTICES

As well-known optical vortex is not supported in conventional SMF. For the guiding and transmission of optical vortex in fiber, the possible candidates include FMF, multimode fiber, and other special fibers [77–88]. Remarkably, different mode sets can be used in optical communications, such as polarization vortices and phase vortices (LG beams, Bessel beams) in free space, eigenmodes and LP modes in fiber. Actually, different mode sets could be converted to each other. For example, the linear combination of TM_{01}, TE_{01}, HE_{21}^{odd}, and HE_{21}^{even} eigenmodes could give LP_{11} modes. Meanwhile, linearly or circularly polarized OAM modes (phase vortex) also could be obtained by the linear combination of TM_{01}, TE_{01}, HE_{21}^{odd}, and HE_{21}^{even} eigenmodes in fiber. Therefore, similar to other mode sets in fiber, one also can use OAM modes in fiber optical communications.

In weakly guiding fiber, different OAM modes have relatively small effective refractive index difference, and they are easy to couple to each other. Thus the mode cross talk

among different OAM modes is unavoidable during long-distance fiber propagation. As a consequence, for OAM multiplexing and transmission in weekly guiding fiber, equalization method such as multiple-input multiple-output (MIMO) digital signal processing (DSP) is needed, which is similar to LP mode multiplexing in FMF. Huang *et al.* demonstrated OAM modes multiplexing and transmission through 5 km FMF using 20 Gbit/s PDM-QPSK signals over OAM_{-1} and OAM_{+1} modes [77]. Channel cross talk was mitigated using 4×4 MIMO DSP with less than 1.5 dB power penalties at a BER of 2×10^{-3}.

In order to reduce mode cross talk and implement MIMO-free OAM multiplexing and transmission in fiber, Zhu *et al.* proposed a new kind of vortex fiber [79]. It has an annular high-index ring with high-index contrast to help with mode stability. It addresses the instability problem by lifting the near-degeneracy of TM_{01}, TE_{01}, and HE_{21} modes. As a result, the difference of effective refractive index (n_{eff}) is larger than 1.8×10^{-4}. By using this annual high-index ring vortex fiber, MIMO-free stable transmission of 80 Gbit/s 16-QAM over two OAM modes on 10 wavelengths (1.6 Tbit/s) through 1.1 km fiber was demonstrated in the experiment [32]. To further increase the number of supported OAM modes, air-core fiber is designed, fabricated, and optimized [81,82]. Large effective refractive index difference enables stable OAM propagation. In addition to air-core fiber, some other kinds of special fiber also can support stable OAM modes (i.e., negligible mode cross talk), such as inverse-parabolic graded-index fiber [83]. Such fiber also offers large effective refractive index separations between modes ($>2.1 \times 10^{-4}$).

We also propose several kinds of special fiber, which could support stable multiple OAM modes [84–86]. Shown in Fig. 24 is a multi-OAM multiring fiber. It consists of seven rings, each supporting 22 modes with 18 OAM ones. The employed high-contrast-index ring structure benefits tight light confinement and large effective refractive index difference of different OAM modes ($>10^{-4}$), featuring both low-level inter-ring cross talk and intermode cross talk over a wide wavelength range (1520–1580 nm). Shown in Fig. 25 is an improved compact (130 μm cladding diameter) trench-assisted multi-OAM multiring fiber with 19 rings, each supporting 22 modes with 18 OAM ones. Using the high-contrast-index ring and trench designs, the trench-assisted multi-OAM multiring fiber features both low-level intermode cross talk and inter-ring crosstalk within a wide wavelength range (1520–1630 nm). Shown in Fig. 26 is a multi-OAM multicore supermode fiber. It consists of equally spaced and circularly arranged multiple cores, in which the core pitch is small enough to support strong coupling OAM supermodes. The designed multi-OAM multicore supermode fiber could transmit multiple OAM modes with favorable performance of low mode coupling, low nonlinearity, and low modal dependent loss.

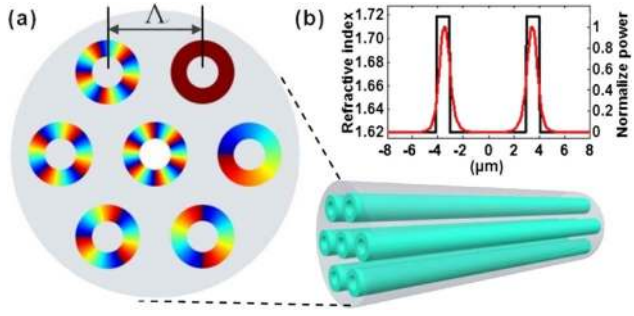

Fig. 24. Schematic illustration of multi-OAM multiring fiber.

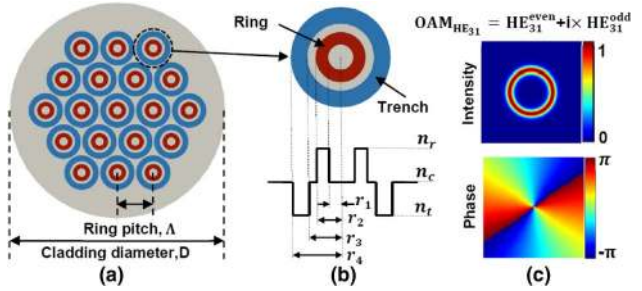

Fig. 25. Schematic illustration and simulated intensity/phase distribution of compact trench-assisted multi-OAM multiring fiber.

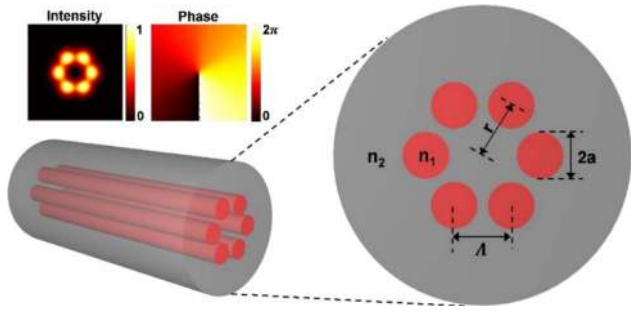

Fig. 26. Schematic illustration and simulated intensity/phase distribution of multi-OAM multicore supermode fiber.

Here we show an example of fiber optical communications using optical vortex modulation [87]. As shown in Fig. 27, at the transmitter, four modes (LP_{01}, LP_{11a}, LP_{11b}, and OAM_{-1}) are converted from a Gaussian beam using four specific phase patterns loaded to the SLM. Note that four modes can be used to represent quaternary numbers ($0 \rightarrow LP_{01}$, $1 \rightarrow LP_{11a}$, $2 \rightarrow LP_{11b}$, and $3 \rightarrow OAM_{-1}$). Thus a quaternary number sequence can be encoded to a time-varying mode sequence for data information transfer in an FMF. After the FMF transmission, at the receiver, the mode sequence is recorded by a camera for analyses. The four transmitted spatial modes (LP_{01}, LP_{11a}, LP_{11b}, and OAM_{-1}) have different intensity distributions. Therefore, one can decode and determine the quaternary number sequence by measuring the intensity distributions of time-varying mode sequence. Using such fiber communications link based on four spatial modes (LP_{01}, LP_{11a}, LP_{11b}, and OAM_{-1}) modulation, successful image transfer through a 1.1 km FMF is demonstrated in the experiment.

For fiber optical communications using optical vortex multiplexing, here we show a proof-of-concept experiment of hybrid MDM and TDM passive optical network (PON) using OAM modes [88]. Figure 28 illustrates OAM-based MDM-TDM-PON architecture. For the downstream link [optical line terminal (OLT) to optical network unit (ONU)], TDM signals from several transmitters ($Tx1 \ldots TxN$) are converted to OAM modes for OAM multiplexing at the OLT side. After propagating through the FMF, OAM demultiplexing is followed. The OAM mode demultiplexed channels are sent into SMF, and signals within specific time slots are received by

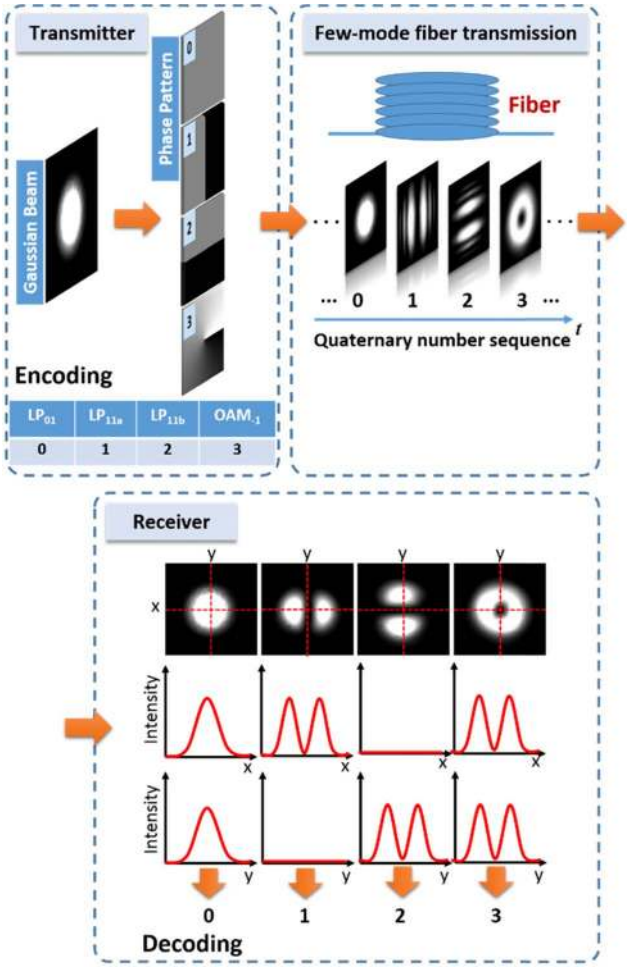

Fig. 27. Schematic illustration of fiber optical communications using modes modulation (LP_{01}, LP_{11a}, LP_{11b}, and OAM_{-1}).

each ONU. The ONUs in one group share a downstream OAM mode, and different ONU groups correspond to different downstream OAM modes. For the upstream link (ONU to OLT), multiuser access to the transmission link is achieved by assigning different time slots to different users (a group of ONUs) in a TDM way. Different groups of ONUs carrying different OAM modes are combined together through OAM multiplexing in an MDM way. After propagation through the FMF, upstream signals from different ONU groups are separated by OAM demultiplexing, followed by each ONU signal detection at the OLT side in specific time slots.

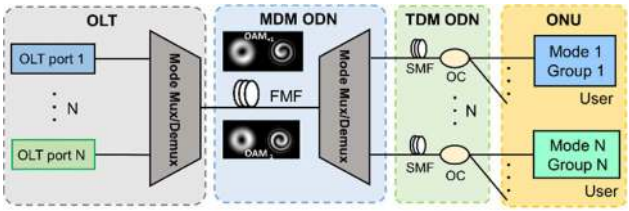

Fig. 28. Schematic illustration of the proposed OAM-based MDM-TDM-PON architecture (hybrid OAM multiplexing and TDM PON). ODN, optical distribution network; Mux/Demux, multiplexing/demultiplexing; OC, optical coupler.

The employed 1.1 km FMF in the experiment is a conventional circular core optical fiber with a step index profile. The radii of the fiber core and cladding are $r_{\text{core}} = 6.35$ μm and $r_{\text{cladding}} = 62.5$ μm, respectively, as shown in Fig. 29(a). The relative refractive index difference ($\Delta = (n_1 - n_2)/n_2$) between the fiber core (n_1) and cladding (n_2) is $\Delta = 0.377\%$. The normalized frequency V of the fiber is 3.23, as shown in Fig. 29(b). Six eigenmodes ($HE_{11}^{even}, HE_{11}^{odd}, TE_{01}, TM_{01}, HE_{21}^{even}, HE_{21}^{odd}$) are supported in the designed and fabricated FMF, which are divided into two mode groups with relatively large effective refractive index difference ($>2.3\times10^{-3}$) between the mode group 1 ($HE_{11}^{even}, HE_{11}^{odd}$) and mode group 2 ($TE_{01}, TM_{01}, HE_{21}^{even}, HE_{21}^{odd}$), as shown in Fig. 29(c). Right circularly polarized OAM_{+1} (OAM_{+1}^{R}) and OAM_{-1} (OAM_{-1}^{R}) modes and left circularly polarized OAM_{+1} (OAM_{+1}^{L}) and OAM_{-1} (OAM_{-1}^{L}) modes can be achieved through proper linear combinations of eigenmodes in mode group 2. In the OAM-based MDM-TDM-PON experiments, OAM_{+1}^{R} and OAM_{-1}^{L} modes are employed.

Figure 30 shows the complex phase patterns used to generate OAM_{+1} and OAM_{-1} modes, measured input and output OAM intensity profiles, and interferograms. One can clearly see the high-quality output OAM modes, indicating that OAM multiplexing transmission in a 1.1 km FMF is successfully demonstrated with favorable transmission performance.

We also measure the BER curves to evaluate downstream and upstream link performance of the OAM-based MDM-TDM-PON. As shown in Fig. 31, bidirectional transmissions with 2.5 Gbaud four-level pulse amplitude modulation (PAM-4) downstream and 2 Gbaud OOK upstream are demonstrated in the experiment. The observed OSNR penalties for downstream and upstream transmissions at a BER of 2×10^{-3} are less than 2.0 and 3.0 dB, respectively.

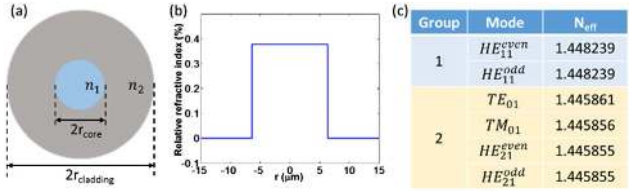

Group	Mode	N_{eff}
1	HE_{11}^{even}	1.448239
	HE_{11}^{odd}	1.448239
2	TE_{01}	1.445861
	TM_{01}	1.445856
	HE_{21}^{even}	1.445855
	HE_{21}^{odd}	1.445855

Fig. 29. (a) Cross section of the FMF. (b) Relative refractive index profile (step-index) of the FMF. (c) Supported six eigenmodes in two mode groups of the FMF.

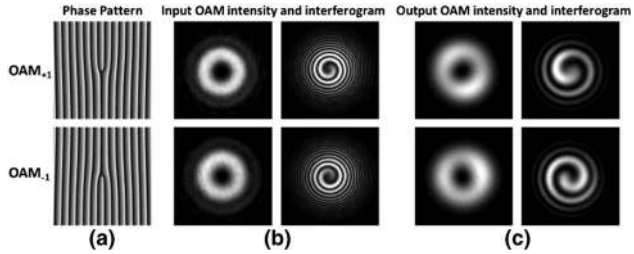

Fig. 30. (a) Complex phase patterns for the generation of OAM_{+1} and OAM_{-1} modes. (b) Measured intensity profiles and interferograms for input OAM modes. (c) Measured intensity profiles and interferograms for output OAM modes after 1.1 km FMF transmission.

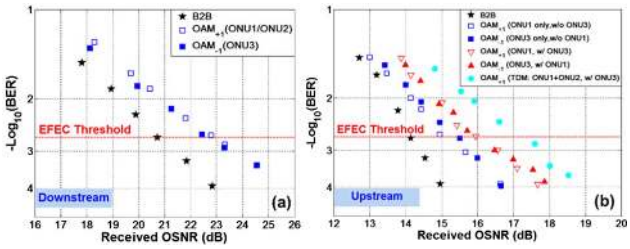

Fig. 31. Measured BER performance for OAM-based MDM-TDM-PON (hybrid OAM multiplexing and TDM PON). (a) Downstream transmission link. (b) Upstream transmission link.

6. DISCUSSION

The optical vortex (polarization vortex, phase vortex) has attracted increasing interest in free-space and fiber optical communications and interconnects. As an alternative mode set, it offers another possible approach to increase the transmission capacity and spectral efficiency by exploiting optical vortex modulation and optical vortex multiplexing. Despite recent advances, there are still lots of challenges to develop optical communications using optical vortices.

For the generation and detection of polarization vortices and phase vortices, photonic integrated devices are of great importance. Although there have been some works on photonic integrated devices with compactness, they are not competitive to commercially available SLM in terms of reconfigurability and efficiency. A valuable goal would be to design, model, and fabricate ultracompact, reconfigurable, broadband, and efficient photonic integrated devices for generating and detecting optical vortices.

For the optical vortex modulation, the modulation speed is challengeable. The commercially available SLM has limited response time. Optical vortex modulation based on SLM is much slower compared with traditional modulation schemes (e.g., OOK, m-QAM) using lithium niobate waveguides. Thus it is valuable to develop high-speed spatial light modulation schemes and devices.

For the optical vortex multiplexing, the great challenge is scalable and efficient (de)multiplexing techniques and devices. Moreover, it is also highly desired that the optical vortex (de)multiplexer is compatible with existing optical communication systems, such as the compatibility with SMF. Similar to the WDM technique and device in a traditional fiber optical transmission system, scalable, efficient, and compatible optical vortex (de)multiplexer would play a key role in optical vortex communications and interconnects.

For the optical vortex communication link, comprehensive characterization of linear and nonlinear free-space and fiber link performance is important [89,90]. In a free-space optical vortex transmission link, diffraction, scattering, divergence, obstacle, and atmospheric turbulence could degrade the transmission performance. Low-density parity-check codes [91] and adaptive optics could provide possible solutions [92,93]. Moreover, MIMO DSP [77] could help to mitigate mode coupling and cross talk. In a fiber optical vortex transmission link, loss, mode cross talk, dispersion, and nonlinearity could degrade the transmission performance and limit the propagation distance. Mode cross talk mitigation techniques in traditional FMF and multimode fiber and improved design and fabrication of special fibers are potential solutions. Meanwhile, optical vortex fiber amplifiers also are challengeable.

In addition to optical transmissions using optical vortex modulation and multiplexing, another important theme of optical communications is optical processing. So far various optical vortex processing techniques have been reported, including optical vortex exchange [29,94], optical vortex switching [95], optical vortex add/drop [96], optical vortex mode filter [97], optical vortex conversion [98], and optical vortex multicasting [99–103]. More grooming optical vortex processing techniques are expected to facilitate robust optical communications using optical vortices. Beyond optical communications using optical vortices, because OAM (i.e., phase vortex) is a natural property of all electromagnetic waves having spiral phase fronts, it is also possible to develop radio and microwave communications using OAM [104,105].

7. CONCLUSION

An optical vortex is an isolated zero intensity point of an optical field. Polarization vortex with polarization singularity and phase vortex with phase singularity are two typical examples of optical vortex. The former features spatially variant polarizations such as radially polarized beam and azimuthally polarized beam with cylindrical symmetry in polarizations, while the latter has a spiral phase front such as LG beam, Bessel beam, and other OAM-carrying beams. Optical vortex is linked to the spatial structure physical dimension of light waves, which has been widely exploited to increase the transmission capacity and spectral efficiency of optical communications. In this paper, we highlight recent advances in optical communications using optical vortices (polarization vortices and phase vortices). We first introduce basic definitions and properties of polarization vortex and phase vortex. We then describe basic concepts of optical communications using polarization vortex modulation, polarization vortex multiplexing, phase vortex modulation, and phase vortex multiplexing. We also present key techniques of polarization vortex and phase vortex generation and (de)multiplexing. After that, we report recent works on free-space and fiber optical communications using polarization vortex modulation and multiplexing as well as phase vortex modulation and multiplexing. We further discuss the challenges and future perspectives of optical communications using optical vortices, including ultracompact, reconfigurable, broadband, efficient photonic integrated devices; high-speed spatial light modulation schemes and devices; scalable, efficient and compatible optical vortex (de)multiplexers, characterization of linear and nonlinear free-space and fiber link performance, and grooming optical vortex processing. We believe optical vortices would find wider promising applications in free-space and fiber optical communications and interconnects.

Funding. National Basic Research Program of China (973 Program) (2014CB340004); National Natural Science Foundation of China (NSFC) (11274131, 11574001, 61222502); National Program for Support of Top-Notch Young Professionals; Program for New Century Excellent Talents in University (NCET) (NCET-11-0182); Wuhan Science and Technology Plan Project (2014070404010201); Open Program from State Key Laboratory of Advanced Optical Communication Systems and Networks (2016GZKF0JT007);

Open Projects Foundation of Yangtze Optical Fiber and Cable Joint Stock Limited Company (YOFC) (SKLD1504).

Acknowledgment. The author would like to gratefully acknowledge S. Li, J. Liu, L. Zhu, J. Du, Y. Zhao, and A. Wang from the Wuhan National Laboratory for Optoelectronics, Huazhong University of Science and Technology; M. Luo, C. Li, D. Xie, Q. Yang, and S.-H. Yu from the State Key Laboratory of Optical Comm. Technologies and Networks; and A. E. Willner from the Department of Electrical Engineering, University of Southern California for insightful discussions.

REFERENCES

1. M. R. Dennis, K. O'Holleran, and M. J. Padgett, "Singular optics: optical vortices and polarization singularities," Prog. Opt. **53**, 293–363 (2009).
2. D. Andrews, *Structured Light and its Applications* (Academic, 2008).
3. Q. Zhang, "Cylindrical vector beams from mathematical concepts to applications," Adv. Opt. Photon. **1**, 1–57 (2009).
4. S. Ramachandran and P. Kristensen, "Optical vortices in fiber," Nanophotonics **2**, 455–474 (2013).
5. M. Padgett, J. Courtial, and L. Allen, "Light's orbital angular momentum," Phys. Today **57**(5), 35–40 (2004).
6. S. Franke-Arnold, L. Allen, and M. Padgett, "Advances in optical angular momentum," Laser Photon. Rev. **2**, 299–313 (2008).
7. A. Yao and M. J. Padgett, "Orbital angular momentum: origins, behavior and applications," Adv. Opt. Photon. **3**, 161–204 (2011).
8. R. Dorn, S. Quabis, and G. Leuchs, "Sharper focus for a radially polarized light beam," Phys. Rev. Lett. **91**, 233901 (2003).
9. H. Kano, S. Mizuguchi, and S. Kawata, "Excitation of surface-plasmon polaritons by a focused laser beam," J. Opt. Soc. Am. B **15**, 1381–1386 (1998).
10. G. M. Lerman, A. Yanai, and U. Levy, "Demonstration of nanofocusing by the use of plasmonic lens illuminated with radially polarized light,"Nano Lett. **9**, 2139–2143 (2009).
11. L. Novotny, M. R. Beversluis, K. S. Youngworth, and T. G. Brown, "Longitudinal field modes probed by single molecules," Phys. Rev. Lett. **86**, 5251–5254 (2001).
12. A. V. Nesterov and V. G. Niziev, "Laser beams with axially symmetric polarization," J. Phys. D **33**, 1817–1822 (2000).
13. M. Meier, V. Romano, and T. Feurer, "Material processing with pulsed radially and azimuthally polarized laser radiation," Appl. Phys. A **86**, 329–334 (2007).
14. Y. I. Salamin, "Electron acceleration from rest in vacuum by an axicon Gaussian laser beam," Phys. Rev. A **73**, 43402 (2006).
15. Q. Zhan, "Trapping metallic Rayleigh particles with radial polarization," Opt. Express **12**, 3377–3382 (2004).
16. M. J. Padgett and R. Bowman, "Tweezers with a twist," Nat. Photonics **5**, 343–348 (2011).
17. K. Dholakia and T. Čižmár, "Shaping the future of manipulation," Nat Photonics **5**, 335–342 (2011).
18. L. Paterson, M. P. MacDonald, J. Arlt, W. Sibbett, P. E. Bryant, and K. Dholakia, "Controlled rotation of optically trapped microscopic particles," Science **292**, 912–914 (2001).
19. N. B. Simpson, K. Dholakia, L. Allen, and M. J. Padgett, "Mechanical equivalence of spin and orbital angular momentum of light: an optical spanner," Opt. Lett. **22**, 52–54 (1997).
20. M. R. Dennis, R. P. King, B. Jack, K. O'Holleran, and M. J. Padgett, "Isolated optical vortex knots," Nat. Phys. **6**, 118–121 (2010).
21. S. Bernet, A. Jesacher, S. Fürhapter, C. Maurer, and M. Ritsch-Marte, "Quantitative imaging of complex samples by spiral phase contrast microscopy," Opt. Express **14**, 3792–3805 (2006).
22. A. Mair, A. Vaziri, G. Weihs, and A. Zeilinger, "Entanglement of the orbital angular momentum states of photons," Nature **412**, 313–316 (2001).
23. J. Leach, B. Jack, J. Romero, A. K. Jha, A. M. Yao, S. Franke-Arnold, D. G. Ireland, R. W. Boyd, S. M. Barnett, and M. J. Padgett, "Quantum correlations in optical angle-orbital angular momentum variables," Science **329**, 662–665 (2010).
24. D. J. Richardson, J. M. Fini, and L. E. Nelson, "Space-division multiplexing in optical fibers," Nat. Photonics **7**, 354–362 2013.
25. G. Li, N. Bai, N. Zhao, and C. Xia, "Space-division multiplexing: the next frontier in optical communication," Adv. Opt. Photon. **6**, 413–487 (2014).
26. R. Ryf, S. Randel, A. H. Gnauck, C. Bolle, A. Sierra, S. Mumtaz, M. Esmaeelpour, E. C. Burrows, R.-J. Essiambre, P. J. Winzer, D. W. Peckham, A. H. McCurdy, and R. Lingle, "Mode-division multiplexing over 96 km of few-mode fiber using coherent 6×6 MIMO processing," J. Lightwave Technol. **30**, 521–531 (2012).
27. B. J. Puttnam, R. Luis, J.-M. Delgado-Mendinueta, J. Sakaguchi, W. Klaus, Y. Awaji, N. Wada, A. Kanno, and T. Kawanishi, "High-capacity self-homodyne PDM-WDM-SDM transmission in a 19-core fiber," Opt. Express **22**, 21185–21191 (2014).
28. R. G. H. van Uden, R. Amezcua Correa, E. Antonio Lopez, F. M. Huijskens, C. Xia, G. Li, A. Schülzgen, H. de Waardt, A. M. J. Koonen, and C. M. Okonkwo, "Ultra-high-density spatial division multiplexing with a few-mode multicore fiber," Nat. Photonics **8**, 865–870 (2014).
29. J. Wang, J.-Y. Yang, I. M. Fazal, N. Ahmed, Y. Yan, H. Huang, Y. X. Ren, Y. Yue, S. Dolinar, M. Tur, and A. E. Willner, "Terabit free-space data transmission employing orbital angular momentum multiplexing," Nat. Photonics **6**, 488–496 (2012).
30. A. E. Willner, J. Wang, and H. Huang, "A different angle on light communications," Science **337**, 655–656 (2012).
31. A. E. Willner, H. Huang, Y. Yan, Y. Ren, N. Ahmed, G. Xie, C. Bao, L. Li, Y. Cao, Z. Zhao, J. Wang, M. P. J. Lavery, M. Tur, S. Ramachandran, A. F. Molisch, N. Ashrafi, and S. Ashrafi, "Optical communications using orbital angular momentum beams," Adv. Opt. Photon. **7**, 66–106 (2015).
32. N. Bozinovic, Y. Yue, Y. Ren, M. Tur, P. Kristensen, H. Huang, A. E. Willner, and S. Ramachandran, "Terabit-scale orbital angular momentum mode division multiplexing in fibers," Science **340**, 1545–1548 (2013).
33. M. Stalder and M. Schadt, "Linearly polarized light with axial symmetry generated by liquid-crystal polarization converters," Opt. Lett. **21**, 1948–1950 (1996).
34. K. S. Youngworth and T. G. Brown, "Focusing of high numerical aperture cylindrical-vector beams," Opt. Express **7**, 77–87 (2000).
35. L. Allen, M. W. Beijersbergen, R. J. C. Spreeuw, and J. P. Woerdman, "Orbital angular momentum of light and the transformation of Laguerre-Gaussian laser modes," Phys. Rev. A **45**, 8185–8189 (1992).
36. P. J. Winzer, "Modulation and multiplexing in optical communication systems," IEEE LEOS Newslett. **23**, 4–10 (2009).
37. Y. Kozawa and S. Sato, "Generation of a radially polarized laser beam by use of a conical Brewster prism," Opt. Lett. **30**, 3063–3065 (2005).
38. M. A. Ahed, A. Voss, M. M. Vogel, and T. Graf, "Multilayer polarizing grating mirror used for the generation of radial polarization in Yb: YAG thin-disk lasers," Opt. Lett. **32**, 3272–3274 (2007).
39. V. G. Niziev, R. S. Chang, and A. V. Nesterov, "Generation of inhomogeneously polarized laser beams by use of a Sagnac interferometer," Appl. Opt. **45**, 8393–8399 (2006).
40. G. Machavariani, Y. Lumer, I. Meir, and S. Jackel, "Spatially-variable retardation plate for efficient generation of radially- and azimuthally-polarized beams," Opt. Commun. **281**, 732–738 (2008).
41. Z. Bomzon, G. Biener, V. Kleiner, and E. Hasman, "Radially and azimuthally polarized beams generated by space-variant dielectric subwavelength gratings," Opt. Lett. **27**, 285–287 (2002).
42. Y. Zhao and J. Wang, "High-base vector beam encoding/decoding for visible-light communications," Opt. Lett. **40**, 4843–4846 (2015).
43. S. Oemrawsingh, J. van Houwelingen, E. Eliel, J. P. Woerdman, E. Verstegen, J. Kloosterboer, and G. Hooft, "Production and characterization of spiral phase plates for optical wavelengths," Appl. Opt. **43**, 688–694 (2004).
44. M. W. Beijersbergen, L. Allen, H. Vanderveen, and J. P. Woerdman, "Astigmatic laser mode converters and transfer of orbital angular momentum," Opt. Commun. **96**, 123–132 (1993).
45. C. Maurer, A. Jesacher, S. Bernet, and M. Ritsch-Marte, "What spatial light modulators can do for optical microscopy," Laser Photon. Rev. **5**, 81–101 (2011).

46. J. Liu and J. Wang, "Demonstration of polarization-insensitive spatial light modulation using a single polarization-sensitive spatial light modulator," Sci. Rep. **5**, 9959 (2015).
47. L. Zhu and J. Wang, "Arbitrary manipulation of spatial amplitude and phase using phase-only spatial light modulators," Sci. Rep. **4**, 7441 (2014).
48. L. Marrucci, E. Karimi, S. Slussarenko, B. Piccirillo, E. Santamato, E. Nagali, and F. Sciarrino, "Spin-to-orbital conversion of the angular momentum of light and its classical and quantum applications," J. Opt. **13**, 064001 (2011).
49. Y. Yan, J. Wang, L. Zhang, J. Y. Yang, I. M. Fazal, N. Ahmed, B. Shamee, A. E. Willner, K. Birnbaum, and S. J. Dolinar, "Fiber coupler for generating orbital angular momentum modes," Opt. Lett. **36**, 4269–4271 (2011).
50. Y. Yan, L. Zhang, J. Wang, J. Y. Yang, I. M. Fazal, N. Ahmed, A. E. Willner, and S. J. Dolinar, "Fiber structure to convert a Gaussian beam to higher-order optical orbital angular momentum modes," Opt. Lett. **37**, 3294–3296 (2012).
51. S. Li, Q. Mo, X. Hu, C. Du, and J. Wang, "Controllable all-fiber orbital angular momentum mode converter," Opt. Lett. **40**, 4376–4379 (2015).
52. T. Su, R. P. Scott, S. S. Djordjevic, N. K. Fontaine, D. J. Geisler, X. Cai, and S. J. B. Yoo, "Demonstration of free space coherent optical communication using integrated silicon photonic orbital angular momentum devices," Opt. Express **20**, 9396–9402 (2012).
53. H. Li, D. B. Phillips, X. Wang, Y.-L. D. Ho, L. Chen, X. Zhou, J. B. Zhu, S. Yu, and X. Cai, "Orbital angular momentum vertical-cavity surface-emitting lasers," Optica **2**, 547–552 (2015).
54. N. Yu, P. Genevet, M. A. Kats, F. Aieta, J. P. Tetienne, F. Capasso, and Z. Gaburro, "Light propagation with phase discontinuities: generalized laws of reflection and refraction," Science **334**, 333–337 (2011).
55. Y. Yang, W. Wang, P. Moitra, I. I. Kravchenko, D. P. Briggs, and J. Valentine, "Dielectric meta-reflectarray for broadband linear polarization conversion and optical vortex generation," Nano Lett. **14**, 1394–1399 (2014).
56. E. Karimi, S. A. Schulz, I. De Leon, V. Qassim, J. Upham, and R. W. Boyd, "Generating optical orbital angular momentum at visible wavelengths using a plasmonic metasurface," Light Sci. Appl. **3**, e167 (2014).
57. X. Cai, J. Wang, M. J. Strain, B. J. Morris, J. Zhu, M. Sorel, J. L. O' Brien, M. G. Thompson, and S. Yu, "Integrated compact optical vortex beam emitters," Science **338**, 363–366 (2012).
58. M. J. Strain, X. Cai, J. Wang, J. Zhu, D. B. Phillips, L. Chen, M. Lopez-Garcia, J. L. O'Brien, M. G. Thompson, M. Sorel, and S. Yu, "Fast electrical switching of orbital angular momentum modes using ultra-compact integrated vortex emitters," Nat. Commun. **5**, 4856 (2014).
59. Z. Zhao, J. Wang, S. Li, and A. E. Willner, "Metamaterials-based broadband generation of orbital angular momentum carrying vector beams," Opt. Lett. **38**, 932–934 (2013).
60. G. Labroille, B. Denolle, P. Jian, P. Genevaux, N. Treps, and J.-F. Morizur, "Efficient and mode selective spatial mode multiplexer based on multi-plane light conversion," Opt. Express **22**, 15599–15607 (2014).
61. G. C. G. Berkhout, M. P. J. Lavery, J. Courtial, M. W. Beijersbergen, and M. J. Padgett, "Efficient sorting of orbital angular momentum states of light," Phys. Rev. Lett. **105**, 153601 (2010).
62. M. Mirhosseini, M. Malik, Z. Shi, and R. W. Boyd, "Efficient separation of the orbital angular momentum eigenstates of light," Nat. Commun. **4**, 2781 (2013).
63. S. Li and J. Wang, "Simultaneous demultiplexing and steering of multiple orbital angular momentum modes," Sci. Rep. **5**, 15406 (2015).
64. T. Lei, M. Zhang, Y. Li, P. Jia, G. N. Liu, X. Xu, Z. Li, C. Min, J. Lin, C. Yu, H. Niu, and X. Yuan, "Massive individual orbital angular momentum channels for multiplexing enabled by Dammann gratings," Light Sci. Appl. **4**, e257 (2015).
65. Y. Yan, Y. Yue, H. Huang, J. Y. Yang, M. R. Chitgarha, N. Ahmed, M. Tur, S. J. Dolinar, and A. E. Willner, "Efficient generation and multiplexing of optical orbital angular momentum modes in a ring fiber by using multiple coherent inputs," Opt. Lett. **37**, 3645–3647 (2012).
66. B. Guan, R. P. Scott, C. Qin, N. K. Fontaine, T. Su, C. Ferrari, M. Cappuzzo, F. Klemens, B. Keller, M. Earnshaw, and S. J. B. Yoo, "Free-space coherent optical communication with orbital angular, momentum multiplexing/demultiplexing using a hybrid 3D photonic integrated circuit," Opt. Express **22**, 145–156 (2014).
67. G. Milione, M. P. J. Lavery, H. Huang, Y. Ren, G. Xie, T. A. Nguyen, E. Karimi, L. Marrucci, D. A. Nolan, R. R. Alfano, and A. E. Willner, "4×20 Gbit/s mode division multiplexing over free space using vector modes and a q-plate mode (de) multiplexer," Opt. Lett. **40**, 1980–1983 (2015).
68. G. Gibson, J. Courtial, and M. J. Padgett, "Free-space information transfer using light beams carrying orbital angular momentum," Opt. Express **12**, 5448–5456 (2004).
69. M. Krenn, R. Fickler, M. Fink, J. Handsteiner, M. Malik, T. Scheidl, R. Ursin, and A. Zeilinger, "Communication with spatially modulated light through turbulent air across Vienna," New J. Phys. **16**, 113028 (2014).
70. J. Du and J. Wang, "High-dimensional structured light coding/decoding for free-space optical communications free of obstructions," Opt. Lett. **40**, 4827–4830 (2015).
71. J. Wang, J.-Y. Yang, I. M. Fazal, N. Ahmed, Y. Yan, B. Shamee, A. E. Willner, K. Birnbaum, J. Choi, B. Erkmen, S. Dolinar, and M. Tur, "Demonstration of 12.8-bit/s/Hz spectral efficiency using 16-QAM signals over multiple orbital-angular-momentum modes," in *European Conference on Optical Communication (ECOC)*, Geneva, Switzerland, (2011), paper We.10.P1.76.
72. J. Wang, J.-Y. Yang, I. M. Fazal, N. Ahmed, Y. Yan, B. Shamee, A. E. Willner, K. Birnbaum, J. Choi, B. Erkmen, S. Dolinar, and M. Tur, "25.6-bit/s/Hz spectral efficiency using 16-QAM signals over pol-muxed multiple orbital-angular-momentum modes," in *Annual Meeting IEEE Photonic Society*, Arlington, VA, (2011), paper WW2.
73. J. Wang, S. Li, C. Li, L. Zhu, C. Gui, D. Xie, Y. Qiu, Q. Yang, and S. Yu, "Ultra-high 230-bit/s/Hz spectral efficiency using OFDM/OQAM 64-QAM signals over pol-muxed 22 orbital angular momentum (OAM) modes," in *Optical Fiber Communications Conference and Exhibition (OFC)*, San Francisco, California, (2014), paper W1H.4.
74. J. Wang, J. Liu, X. Lv, L. Zhu, D. Wang, S. Li, A. Wang, Y. Zhao, Y. Long, J. Du, X. Hu, N. Zhou, S. Chen, L. Fang, and F. Zhang, "Ultra-high 435-bit/s/Hz spectral efficiency using N-dimensional multiplexing and modulation link with pol-muxed 52 orbital angular momentum (OAM) modes carrying Nyquist 32-QAM signals," in *European Conference on Optical Communication (ECOC)*, (2015), paper Th.2.5.4.
75. H. Huang, G. Xie, Y. Yan, N. Ahmed, Y. Ren, Y. Yue, D. Rogawski, B. I. Erkmen, K. M. Birnbaum, S. J. Dolinar, M. P. J. Lavery, M. J. Padgett, M. Tur, and A. E. Willner, "100 Tbit/s free-space data link enabled by three-dimensional multiplexing of orbital angular momentum, polarization, and wavelength," Opt. Lett. **39**, 197–200 (2014).
76. J. Wang, S. Li, M. Luo, J. Liu, L. Zhu, C. Li, D. Xie, Q. Yang, S. Yu, J. Sun, X. Zhang, W. Shieh, and A. E. Willner, "N-dimensional multiplexing link with 1.036-Pbit/s transmission capacity and 112.6-bit/s/Hz spectral efficiency using OFDM-8QAM signals over 368 WDM pol-muxed 26 OAM modes," in *European Conference on Optical Communication (ECOC)*, Cannes, France, (2014), paper Mo.4.5.1.
77. H. Huang, G. Milione, M. P. J. Lavery, G. Xie, Y. Ren, Y. Cao, N. Ahmed, T. A. Nguyen, D. A. Nolan, M.-J. Li, M. Tur, R. R. Alfano, and A. E. Willner, "Mode division multiplexing using an orbital angular momentum mode sorter and MIMO-DSP over a graded-index few-mode optical fiber," Sci. Rep. **5**, 14931 (2015).
78. L. Zhu, A. Wang, S. Chen, J. Liu, C. Du, Q. Mo, and J. Wang, "Experimental demonstration of orbital angular momentum (OAM) modes transmission in a 2.6 km conventional graded-index multimode fiber assisted by high efficient mode-group excitation," in *Optical Fiber Communication Conference (OFC)*, Anaheim, California, (2016), paper W2A.32.
79. L. Zhu, J. Liu, Q. Mo, C. Du, and J. Wang, "Encoding/decoding using superpositions of spatial modes for image transfer in km-scale few-mode fiber," Opt. Express **24**, 16934–16944 (2016).
80. S. Ramachandran, P. Kristensen, and M. Yan, "Generation and propagation of radially polarized beams in optical fibers," Opt. Lett. **34**, 2525–2527 (2009).

81. G. Wong, M. Kang, H. Lee, F. Biancalana, C. Conti, T. Weiss, and P. St.J. Russell, "Excitation of orbital angular momentum resonances in helically twisted photonic crystal fiber," Science **337**, 446–449 (2012).
82. C. Brunet, P. Vaity, Y. Messaddeq, S. LaRochelle, and L. A. Rusch, "Design, fabrication and validation of an OAM fiber supporting 36 states," Opt. Express **22**, 26117–26127 (2014).
83. P. Gregg, P. Kristensen, and S. Ramachandran, "Conservation of orbital angular momentum in air-core optical fibers," Optica **2**, 267–270 (2015).
84. B. Ung, P. Vaity, L. Wang, Y. Messaddeq, L. A. Rusch, and S. LaRochelle, "Few-mode fiber with inverse-parabolic graded-index profile for transmission of OAM-carrying modes," Opt. Express **22**, 18044–18055 (2014).
85. S. Li and J. Wang, "Multi-orbital-angular-momentum multi-ring fiber for high-density space-division multiplexing," IEEE Photon. J. **5**, 7101007 (2013).
86. S. Li and J. Wang, "A compact trench-assisted multi-orbital-angular-momentum multi-ring fiber for ultrahigh-density space-division multiplexing (19 rings × 22 modes)," Sci. Rep. **4**, 3853 (2014).
87. S. Li and J. Wang, "Supermode fiber for orbital angular momentum (OAM) transmission," Opt. Express **23**, 18736–18745 (2015).
88. A. Wang, L. Zhu, J. Liu, C. Du, Q. Mo, and J. Wang, "Demonstration of hybrid orbital angular momentum multiplexing and time-division multiplexing passive optical network," Opt. Express **23**, 29457–29466 (2015).
89. S. Li and J. Wang, "Performance evaluation of analog signal transmission in an orbital angular momentum multiplexing system," Opt. Lett. **40**, 760–763 (2015).
90. J. Liu, S. M. Li, J. Du, C. Klitis, C. Du, Q. Mo, M. Sorel, S. Yu, X. Cai, and J. Wang, "Performance evaluation of analog signal transmission in an integrated optical vortex emitter to 3.6-km few-mode fiber system," Opt. Lett. **41**, 1969–1972 (2016).
91. I. B. Djordjevic and M. Arabaci, "LDPC-coded orbital angular momentum (OAM) modulation for free-space optical communication," Opt. Express **18**, 24722–24728 (2010).
92. Y. Ren, G. Xie, H. Huang, C. Bao, Y. Yan, N. Ahmed, M. P. J. Lavery, B. I. Erkmen, S. Dolinar, M. Tur, M. A. Neifeld, M. J. Padgett, R. W. Boyd, J. H. Shapiro, and A. E. Willner, "Adaptive optics compensation of multiple orbital angular momentum beams propagating through emulated atmospheric turbulence," Opt. Lett. **39**, 2845–2848 (2014).
93. S. Li and J. Wang, "Compensation of a distorted N-fold orbital angular momentum multicasting link using adaptive optics," Opt. Lett. **41**, 1482–1485 (2016).
94. J. Liu, L. Zhu, A. Wang, S. Li, S. Chen, C. Du, Q. Mo, and J. Wang, "All-fiber pre- and post-data exchange in km-scale fiber-based twisted lights multiplexing," Opt. Lett. **41**, 3896–3899 (2016).
95. Y. Yue, H. Huang, N. Ahmed, Y. Yan, Y. Ren, G. Xie, D. Rogawski, M. Tur, and A. E. Willner, "Reconfigurable switching of orbital-angular-momentum-based free-space data channels," Opt. Lett. **38**, 5118–5121 (2013).
96. H. Huang, Y. Yue, Y. Yan, N. Ahmed, Y. Ren, M. Tur, and A. E. Willner, "Liquid-crystal-on-silicon-based optical add/drop multiplexer for orbital-angular-momentum-multiplexed optical links," Opt. Lett. **38**, 5142–5145 (2013).
97. H. Huang, Y. Ren, G. Xie, Y. Yan, Y. Yue, N. Ahmed, M. P. J. Lavery, M. J. Padgett, S. J. Dolinar, M. Tur, and A. E. Willner, "Tunable orbital angular momentum mode filter based on optical geometric transformation," Opt. Lett. **39**, 1689–1692 (2014).
98. L. Fang and J. Wang, "Flexible generation/conversion/exchange of fiber-guided orbital angular momentum modes using helical gratings," Opt. Lett. **40**, 4010–4013 (2015).
99. Y. Yan, Y. Yue, H. Huang, Y. Ren, N. Ahmed, M. Tur, S. J. Dolinar, and A. E. Willner, "Multicasting in a spatial division multiplexing system based on optical orbital angular momentum," Opt. Lett. **38**, 3930–3933 (2013).
100. L. Zhu and J. Wang, "Simultaneous generation of multiple orbital angular momentum (OAM) modes using a single phase-only element," Opt. Express **23**, 26221–26233 (2015).
101. J. Du and J. Wang, "Design of on-chip N-fold orbital angular momentum multicasting using V-shaped antenna array," Sci. Rep. **5**, 9662 (2015).
102. S. Li and J. Wang, "Adaptive power-controllable orbital angular momentum (OAM) multicasting," Sci. Rep. **5**, 9677 (2015).
103. L. Zhu and J. Wang, "Demonstration of obstruction-free data-carrying N-fold Bessel modes multicasting from a single Gaussian mode," Opt. Lett. **40**, 5463–5466 (2015).
104. F. Tamburini, E. Mari, A. Sponselli, B. Thidé, A. Bianchini, and F. Romanato, "Encoding many channels on the same frequency through radio vorticity: first experimental test," New J. Phys. **14**, 033001 (2012).
105. Y. Yan, G. Xie, M. P. J. Lavery, H. Huang, N. Ahmed, C. Bao, Y. Ren, Y. Cao, L. Li, Z. Zhao, A. F. Molisch, M. Tur, M. J. Padgett, and A. E. Willner, "High-capacity millimetre-wave communications with orbital angular momentum multiplexing," Nat. Commun. **5**, 4876 (2014).